Molecular Neurobiology (2019) 56:7420–7432
https://doi.org/10.1007/s12035-019-1597-z

Bispecific Antibody Fragment Targeting APP and Inducing α-Site Cleavage Restores Neuronal Health in an Alzheimer's Mouse Model

Ping He[1] · Wei Xin[1] · Philip Schulz[1] · Michael R. Sierks[1]

Received: 6 August 2018 / Accepted: 2 April 2019 / Published online: 30 April 2019

Abstract

The amyloid β (Aβ) peptide, correlated with development of Alzheimer's disease (AD), is produced by sequential proteolytic cleavage of the amyloid precursor protein (APP) by β- and γ-secretases. Alternative proteolytic cleavage of APP by α-secretase prevents formation of Aβ peptide and produces a neuroprotective protein, a soluble fragment of APPα (sAPPα). We previously generated a single-chain variable domain antibody fragment (scFv) that binds APP at the β-secretase cleavage site and blocks cleavage of APP (iBsec1), and a second scFv which has been engineered to have α-secretase-like activity that increases α-secretase cleavage of APP (Asec1a) and showed that a bispecific antibody (Diab) combining both iBsec1 and Asec1a constructs protects mammalian cells from oxidative stress. Here, we show that the diabody is an effective therapeutic agent in a mouse model of AD. An apolipoprotein B (ApoB) binding domain peptide was genetically added to the diabody to facilitate transfer across the blood-brain barrier, and a recombinant human adeno-associated virus 2/8 (rAAV2/8) was used as a vector to express the gene constructs in a APP/PS1 mouse model of AD. The diabody increased levels of sAPPα, decreased Aβ deposits and levels of oligomeric Aβ, increased neuronal health as indicated by MAP2 and synaptophysin staining, increased hippocampal neurogenesis, and most importantly dramatically increased survival rates compared with untreated mice or mice treated only with the β-secretase inhibitor. These results indicate that altering APP processing to inhibit β-site activity while simultaneously promoting α-secretase processing provides substantially increased neuronal benefits compared with inhibition of β-secretase processing alone and represents a promising new therapeutic approach for treating AD.

Keywords Single-chain antibody · α-Secretase · β-Secretase · Amyloid precursor protein · Neuron · Alzheimer's disease · Transgenic mice

Introduction

Amyloid β (Aβ) accumulation has been strongly correlated with AD. Therefore, both inhibiting Aβ production and facilitating its clearance represent promising therapeutic strategies for treating AD. Aβ peptide is produced by proteolytic cleavage of the amyloid precursor protein (APP) [1]. Three proteases control the processing of APP into Aβ: α-secretase cleaves APP between what would be residues 16(Lys) and 17(Leu) of Aβ, releasing a soluble α fragment of APP (sAPPα) and leaving a non-amyloidogenic membrane-bound protein; alternatively, β-secretase can cleave APP to form the amino terminal of Aβ, releasing a slightly shorter soluble β fragment of APP molecule (sAPPβ) and leaving a potentially amyloidogenic membrane-bound protein; γ-secretase cleaves the membrane-bound fragment at the C-terminal of Aβ to release the amyloidogenic Aβ protein. The β-site APP cleaving enzyme-1 (BACE-1) is the predominant enzyme involved in β-secretase processing of APP and is a primary therapeutic target for treatment of AD. Inhibitors of β- or γ-secretase are currently being pursued as potential therapeutics for AD (reviewed in [2–5]).

Decreasing Aβ production by inhibiting β- or γ-secretase activity is a promising therapeutic approach though each of these enzymes also has other biological functions than processing APP. A recent clinical trial to inhibit γ-secretase activity using semagacestat was halted as it caused a decrease in cognitive ability and an increase in skin cancer risk [6]. Inhibiting BACE-1 activity is also a promising avenue, and numerous small-molecule inhibitors such as OM99-2 have

Electronic supplementary material The online version of this article (https://doi.org/10.1007/s12035-019-1597-z) contains supplementary material, which is available to authorized users.

✉ Michael R. Sierks
sierks@asu.edu

[1] Department of Chemical Engineering, Arizona State University, ECG301- 501 Tyler Mall, Tempe, AZ 85281-6106, USA

been developed [7]. However, while decreasing BACE-1 activity decreases processing of APP to Aβ, it can also have detrimental effects since BACE-1 has other substrates such as β-subunit of voltage-gated sodium channels [8], NRG-1 involving in myelination [9], and low-density lipoprotein receptor–related protein (LRP) [10]. BACE-1 knockout mice show signs of hypomyelination [11] and impaired synaptic function [12]. A clinical trial of a BACE-1 inhibitor was recently halted early because there were little benefit and increased risk of unwanted side effects [13]. Since BACE-1 has physiologically important activity beyond APP cleavage, a more effective therapeutic strategy for AD would be to selectively block BACE-1 activity toward the APP cleavage site without interfering with BACE-1 activity toward other substrates. One way to accomplish this goal is to bind the APP substrate at the BACE-1 cleavage site essentially blocking BACE-1 processing of APP. Since the BACE-1 cleavage site includes the N-terminal of Aβ, which is an immunodominant epitope [14], binding to APP should ideally occur just upstream of the Aβ sequence to avoid also binding soluble Aβ. This was our rationale in the development of iBsec1, a nanobody which selectively inhibits BACE-1 processing of APP without binding Aβ [15]. In cell models of AD, iBsec1 binds APP on the cell surface, reduces toxicity induced by APP overexpression, and dramatically reduces both intracellular and extracellular Aβ levels by over 50% [15]. The iBsec1 nanobody therefore represents a promising method to inhibit Aβ production from APP.

Increasing non-amyloidogenic processing of APP by promoting α-secretase cleavage of APP is another promising pathway to lower Aβ levels [16]. We engineered a proteolytic nanobody to selectively cleave Aβ at its α-secretase site. The proteolytic nanobody Asec1a prevents aggregation of monomeric Aβ, inhibits further aggregation of pre-formed oligomeric Aβ aggregates, and reduces Aβ-induced cytotoxicity toward a human neuroblastoma cell line and in cells overexpressing APP [17, 18] and promotes non-amyloidogenic processing of APP [17]. The Asec1a proteolytic nanobody was engineered to selectively cleave APP and not other substrates with similar sequences [17].

Here, we propose an innovative therapeutic approach for treating AD by combining the iBsec1 scFv with the Asec1a proteolytic scFv to generate a bispecific construct or diabody that is designed to very selectively decrease amyloidogenic processing of APP by inhibiting BACE-1 activity toward APP, while simultaneously promoting non-amyloidogenic processing of APP by increasing α-secretase activity. The two components should act synergistically since the nanobody targeting the β-secretase site of APP will position the proteolytic nanobody very close to the α-secretase site, increasing its activity by greatly increasing the effective APP concentration surrounding the proteolytic nanobody. We showed that a bispecific tandem scFv construct (Diab) expressing both iBsec-1 and Asec1a effectively lowered Aβ levels and increased sAPPα levels in cell models of AD [19]. Here, we show that the Diab construct also is an effective therapeutic for treating a mouse model of AD. We added the LDLR-binding domain of apoB to the construct to facilitate transfer across the blood-brain barrier [20, 21]. The Diab and iBsec1 construct alone were both tested in an APP/PS1 mouse model of AD using an AAV vector to express the gene construct. While both the iBsec1 and Diab constructs reduced plaque loads to similar extents, the Diab also increased sAPPα levels, improved neuronal health, and dramatically increased survival compared with iBsec1 by itself suggesting that tailoring APP processing by simultaneously inhibiting β-secretase processing of APP and promoting α-secretase processing is a promising therapeutic approach for treating both AD and other diseases such as Down's syndrome which overexpress APP.

Materials and Methods

Construction of Recombinant Human Adenoid Virus Vectors The cDNA constructs of the iBsec1 and Diab genes were amplified by PCR and then cloned into the pFBAAVCAG vector (G0345, Viral Vector Core Facility, University of Iowa) including an ApoB domain producing the vectors rAAV-scFv-Diab and rAAV-scFv-Bsec, with rAAV-GFP as control. FLAG tag was placed at the C-terminal ends of scFv as a marker.

Recombinant Adeno-associated Virus Preparation The vectors AAV2/8 containing plasmids pAAV-scFv were generated through triple transfection into HEK293 cells (Viral Vector Core Facility, University of Iowa). The vector encoding scFv iBsec1 reacts with the β-site of APP while the one encoding the tandem scFv construct reacts with both β- and α-sites of APP. A control rAAV encoding GFP was similarly prepared to the construct without ApoB gene. The viral particles were released and the titers of rAAV virions containing the vector genomes were determined by a quantitative dot-blot assay (Viral Vector Core Facility, University of Iowa).

Experimental Animals and Administration of rAAV-scFvs Female mice at 1-month age (wild type and controls) were purchased from Jackson Laboratory (Bar Harbor, ME). The transgenic mouse model is generated on a C57BL/6J genetic background that expresses KM670/671NL Swedish mutation of human amyloid precursor protein (APPswe) and presenilin1 lacking exon9 (PSEN1dE9) (APP/PS1 mice, catalog: 34832) [22]. The mice showed cerebral amyloidosis onset of 6–8 weeks and amyloid-associated pathologies include dystrophic synaptic buttons, robust gliosis, and microglia number increase and reaction [23]. All protocols for animal use were approved by the Institutional Animal Care and Use

Committee (IACUC) of the Arizona State University at Tempe, Arizona. Experiments described here were carried out in accordance with good animal practice following NIH recommendations. The littermates of APP/PS1 mice at age of 1 month were randomly assigned to three groups for the scFv application: rAAV-GFP (as positive vehicles, $n = 20$), rAAV-scFv-Diab ($n = 10$), rAAV-scFv-Bsec ($n = 10$) as well as rAAV-GFP in wild-type mice ($n = 10$) as negative controls. APP/PS1 mice were subjected to a single intraperitoneal injection of rAAV-scFv (3.0×10^{10} vg/mouse). As controls, age-matched APP/PS1 and WT mice received the same amount of rAAV-GFP administration. The experimental mice survived 9 months as rAAV-GFP Tg mice ($n = 10$), rAAV-scFv-Diab ($n = 9$), and rAAV-scFv-Bsec ($n = 6$) as well as rAAV-GFP WT mice ($n = 10$). The mice at the age of 10 month were sacrificed and the tissues were harvested.

Level Analysis of scFv in the Brain Neocortical tissues were harvested from the APP/PS1 mice receiving rAAV2/8 administration for 9 months ($n = 4$ per group). The brain tissue was homogenized in a homogenization buffer. Multiple tag (catalog: M0101, GenScript, Piscataway, NJ), a designed fusion protein and molecular weight of ~ 40 kDa on SDS-PAGE, contains FLAG sequence DYKDDDDK. Correspondingly, the molecular weight was calculated as scFv Bsec FLAG ~ 30 kDa and scFv diabody FLAG ~ 60 kDa. The protein concentration was measured using a capture ELISA protocol. Monoclonal anti-FLAG antibody (Sigma-Aldrich, St. Louis, MO) was applied. The readout values were normalized to picogram per milligram of brain tissues.

Tissue Fixation and Section Nine months after the rAAV2/8 injection, mice were euthanized with isoflurane and perfused with cold 0.1 M phosphate buffer (PB) including 10 U of heparin sodium (AK3004, Akron Biotech). The brain tissues were quickly removed and mid-incised. The right hemispheres were frozen on dry ice following − 80 °C storage for further biochemistry and the left ones were fixed in 4% (*w*/*v*) paraformaldehyde in 0.1 M PB for 48 h at room temperature. The fixed hemi-brains were then dehydrated with 30% sucrose in 0.1 M PBS for 24 h at 4 °C. The brain tissues were embedded in Tissue-Tek OCT compound and frozen − 18 °C in a cryostat (Leica, CM3000). The blocks were sagittally sectioned on a freezing stage (30 μm thick) at a temperature of − 18 °C in a serial manner. The serial free-floating sections were stored in 0.1 M PBS at 4 °C for further use.

Congo Red Staining Congo red (C6277, Sigma-Aldrich, St. Louis, MO) was diluted in 70% ethanol with stirring overnight. Prior to incubation, the solution was filtered. The sections were incubated for 20 min at room temperature. After washing, the sections were counterstained to show cell nuclei with hematoxylin (Sigma-Aldrich, St. Louis, MO).

DAB Chromogenic Immunohistochemistry Immunostaining was performed as described previously [24, 25]. To eliminate endogenous peroxidase of the brain tissues, the brain sections through the hippocampus at the interval of 480 μm ($n = 10$ or 11 serial sections for each mouse) were treated with 1% H_2O_2 in − 20 °C methanol for 10 min. After washing with 0.1 M PBS (pH 7.4), to prevent non-specific protein binding, sections were blocked with 10% normal goat or horse serum (matching the secondary antibody host species) in 0.1 M PBS with 0.05% Triton X-100 for 30 min at room temperature. For detection of Aβ load, the sections were then incubated with a monoclonal antibody 6E10 (1:2000, catalog: SIG-39320, Covance) in 0.1 M PBS with slow shaking on a horizontal shaker stage overnight at 4 °C. The sections were rinsed in 0.1 M PBS and incubated with biotinylated secondary antibody of horse anti-mouse IgG in 10% horse serum for 1 h at room temperature. Following washing with 0.1 M PBS, a Vectastain kit including avidin-biotin complex (ABC) peroxidase (Vector Laboratories, Burlingame, CA) was used for 30 min at room temperature. The amyloid plaques were visualized with a kit of the 3,3′-diaminobenzidine (DAB) as a substrate (Vector Laboratories). For negative controls, slices were processed deleting primary antibody. These sections were counterstained with hematoxylin (Sigma-Aldrich, St. Louis, MO) and dehydrated with gradual degree of ethanol at percentage of 50, 75, 90, and 100 and cleared with xylene (catalog: 23400, Electric Microscopy Sciences) and coverslip fixed with permount mounting medium (catalog: 17986-01, Electric Microscopy Sciences).

Double Immunofluorescent Staining Immunofluorescent staining was performed as described previously [25, 26]. To prevent non-specific protein binding, the slices were blocked with 10% normal goat in 0.1 M PBS with 0.05% Triton X-100 for 30 min at room temperature. To observe changes in neuroinflammation induced by scFv administration, the sections were incubated with primary antibodies in 0.1 M PBS with slow shaking on a horizontal shaker stage overnight at 4 °C: rabbit anti-ionized calcium-binding adaptor molecule 1 (Iba1) antibody (1:500, catalog: 019-19741, Wako, Richmond, VA), rabbit anti-glial fibrillary acidic protein (GFAP, 1:10,000, Z0334, Dako), monoclonal antibody 6E10 (1:2000, SIG-39320, Covance), rabbit anti-adeno-associated virus capsid VP3 (AAV2, 1:500, catalog: NB100-93575, Novus Biologicals, Centennial, CO). The sections were rinsed in 0.1 M PBS and incubated with fluorescent-conjugated secondary antibody of goat anti-mouse or rabbit IgG in 10% goat serum for 30 min at room temperature. Following washing with 0.1 M PBS, to block non-specific fluorescence of the endogenous lipofuscin, the sections were blocked with 0.3% Sudan Black in 70% alcohol for 3 min at room temperature. Finally, the slices were mounted on glass slides and coverslips fixed with antifade Fluoro-Gel II including 4′,6-diamidino-2-

phenylindole (DAPI) labeling all of cell nuclei (Electric Microscopy Sciences).

Immunoblot Analysis The cortex tissue was homogenized in PBS buffer (Sigma-Aldrich, St. Louis, MO), which contains 1% Nonidet P-40 (Calbiochem, Billerica, MA), and protease and phosphatase inhibitor cocktails (Roche, Pleasanton, CA). The homogenate was centrifuged at 14,000 rpm for 20 min. The protein concentration of supernatants was assayed with a BCA protein assay kit (Pierce Biotechnology, Rockford, IL). The supernatants of the homogenates from the cortex (50 μg) were mixed with 2× Laemmli sample buffer (Bio-Rad, Hercules, CA) with 0.001% bromphenol blue. The samples were heated at 75 °C for 10 min and loaded to 10% Tris-HCl gradient SDS-PAGE. The isolated proteins were electrotransferred to 0.45 μm of nitrocellulose membranes (Millipore, Bedford, MA). APP fragment proteins on the membranes were detected using mouse anti-soluble APP β fragment of Swedish mutation (sAPPβ-sw, clone: 6A1, catalog: 10321, IBL, Minneapolis, MN), mouse anti-soluble APP α fragment of Swedish mutation (sAPPα, clone: 2B3, catalog: 11088, IBL), rabbit anti-APP full length (clone: 22C11, catalog: MAB348, Burlington, MA), and rabbit anti-β-secretase 1 (BACE1, catalog: B0681, Sigma-Aldrich). The membrane was then incubated with secondary antibodies conjugated with horseradish peroxidase (Santa Cruz Biotechnology, Santa Cruz, CA) and visualized by an enhanced DAB system (Sigma-Aldrich) according to the manufacturers' instructions. Semi-quantification was used to analyze with a Versadoc XL imaging apparatus (Bio-Rad). β actin levels were used as loading controls.

Quantification of Immunostaining Structures The immunostained structures such as amyloid β deposits, reactive/activated glial cells, dendrites, and new neurons were measured [24]. The microscope BX51T-PHD-J11 (Olympus, Tokyo, Japan) with objective × 20 and × 40 PL FLUOTAR was employed. Histomorphotometry images were captured by a DEI-470 digital camera (Optronics, Goleta, CA, USA) within the defined areas from each section. Ten to 11 serial sagittal brain sections through the hippocampus per mouse, each separated by an approximately 480-μm interval, were employed from each mouse. Analysis for the quantification was performed using the ImageJ analysis software (NIH). For immunopositive structures, a semi-automated red-green-blue color threshold was applied to determine the optimal segmentation of threshold setting. Using deconvolution method, we subtracted the background counterstain to determine the specific mean immunostaining. Both the cortex and hippocampus were seen in all the sagittal brain sections. An average value of immunostaining areas was expressed as a percentage of total area in the cortex or the hippocampus. For amyloid plaque number, we counted all of the positive staining of the cortex and the hippocampus on each section and expressed as number per section. For the number of newborn neuron, we counted all of doublecortin positive staining in the subgranular zone of the dentate gyrus in the hippocampus on each section and expressed as number per section. An average value was determined for each group and data were expressed as mean ± SEM (standard error of the mean) in the figures of the bar graph.

Statistical Analysis We performed statistical analysis using SPSS 13.0 software (SPSS, Inc., Chicago, IL, USA). Two-way repeated measures of analysis of variance (ANOVA) and Student-Newman-Keuls q or Dunnett t test were used to determine the intergroup significant difference. $p < 0.05$ was considered statistically significant.

Results

Brain Expression of Protein scFv

To exclude the possibility that the virus crossed the blood-brain barrier into the brain, brain tissue sections were immunostained with antibody against AAV2. Not surprisingly, negative staining of AAV2 was visualized in all of the rAAV2/8 vector administration groups (Supplemental Figure 1B). These data indicate little if any active virus in the brain after the IP injections. To verify the role of the ApoB fragment in crossing the blood-brain barrier (BBB), we examined the brain sections under a fluorescence microscope and found negative fluorescence of GFP in WT and Tg mice receiving rAAV-GFP without the ApoB gene (Fig. 1a). As expected, negative results were observed in the Tg mice receiving rAAV-scFv-Diab and rAAV-scFv-Bsec (Supplemental Figure 1D).

Next, we observed whether scFv with apoB tag originating in the liver could enter the brain tissue of mice receiving rAAV delivery. The immunostaining was performed with antibody against FLAG. We found that immunopositive FLAG was localized in the cytoplasm and membrane of neuro-like cells in the mice administered with rAAV-scFv-Diab and rAAV-scFv-Bsec injections (Fig. 1b) but negative staining in WT and Tg mice receiving rAAV-GFP injections (Supplemental Figure 1F). We also measured scFv levels in the brain tissue. A control protein containing the FLAG tag was diluted and used as a standard. The scFv-FLAG levels were measured and normalized to picogram/milligram of the cortical tissue. ScFv levels were ~ 80 pg/mg of neocortex tissue of the mice administered with either rAAV-scFv-Bsec or rAAV-scFv-Diab, but levels as expected were not detectable in WT and Tg mice receiving rAAV-GFP (Fig. 1c). These results indicate that both scFv-Diab and scFv-Bsec could successfully cross the BBB into the brain.

scFv-Diab Administration Elevated sAPPα Levels in APP/PS1 Mice

The APP/PS1 mice were injected with either AAV-GFP, AAV-Bsec, or AAV-Diab. After 9 months, the mice were sacrificed and brain tissue harvested for analyses. To determine the effects of iBsec1 and Diab administration on APP processing, APP cleavage fragments were measured by Western blot (Fig. 2a). There were not any significant differences in expression of human APP levels in the transgenic mice with or without scFv application and no expression of human APP in the WT mice (Fig. 2b). The sAPPα levels were elevated in both the iBsec1- and Diab-treated mice compared with GFP control (Fig. 2a, b, $^{**}p < 0.01$ and $^{***}p < 0.001$), and statistically higher in the Diab-treated mice compared with the scFv-Bsec-treated mice (Fig. 2b, $^{\&\&\&}p < 0.001$). There was also a significant decrease in sAPPβ levels in both the scFv-Bsec- and scFv-Diab-treated mice compared with the GFP control group (Fig. 2a, b, $^{*}p < 0.05$). The decrease in sAPPβ levels was not due to change in expression of BACE1 enzyme levels as this remained constant in the different treatment groups (Fig. 2).

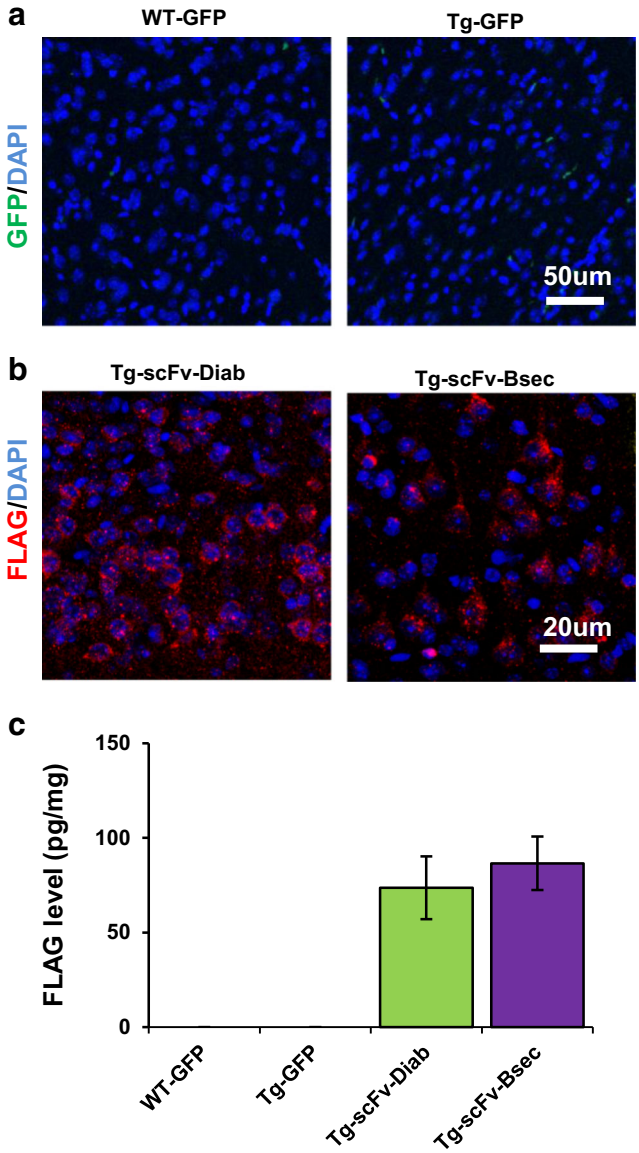

Fig. 1 Protein level of scFv in the brains of mice with the rAAV delivery. **a** Representative microphotoimages showed the brain localization of green fluorescent protein (GFP) in the brains of mice receiving the IP injection of rAAV-GFP. Counterstaining by DAPI (blue). **b** Representative microphotoimages showed the brain localization of scFv labeled with FLAG tag (red) in the brains of mice receiving the IP injection of rAAV-scFv-Diab-FLAG and rAAV-scFv-Bsec-FLAG. **c** scFv concentration was measured by rabbit anti-FLAG antibody by ELISA. Data were expressed as pg/mg of the cortex tissue following the application of scFv-Diab ($n = 4$), scFv-Bsec ($n = 4$), Tg-GFP ($n = 4$), and WT-GFP ($n = 4$)

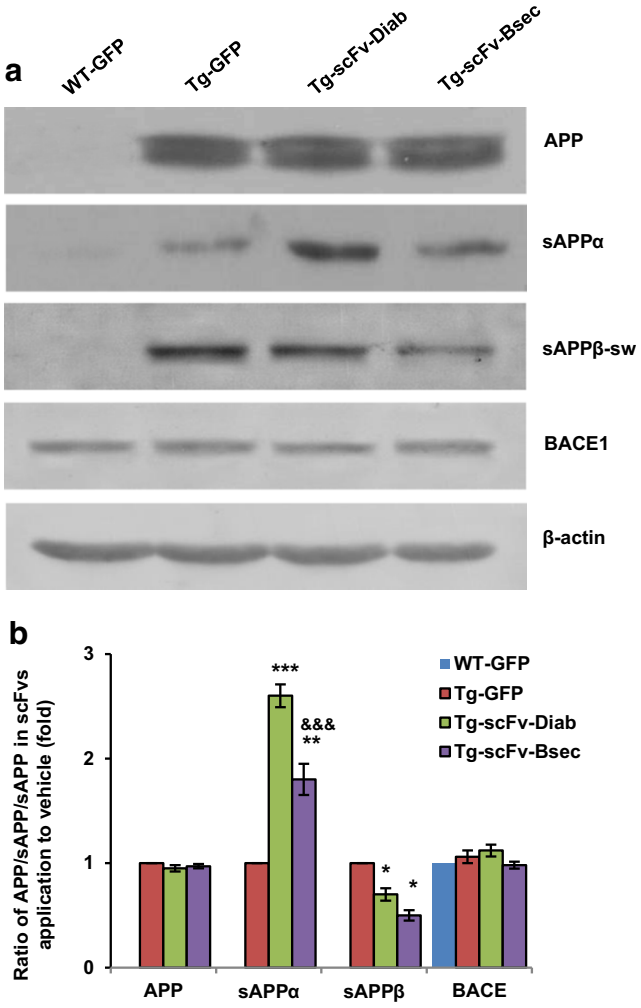

Fig. 2 Soluble APP fragments in the brains of APP/PS1 mice. **a** Representative data showing APP, sAPPα, sAPPβ, and BACE1 levels in the cortex by Western blot. **b** Normalized to age-matched WT, semi-quantification showed the total amount of APP, sAPPα, sAPPβ and BACE1 in the cortex among the mice following the application of scFv-Diab ($n = 5$), scFv-Bsec ($n = 5$), Tg-GFP ($n = 5$), and WT-GFP ($n = 5$). $^{*}p < 0.05$, $^{**}p < 0.01$, $^{***}p < 0.001$ to vehicle Tg-GFP mice; $^{\&\&\&}p < 0.001$ to Tg-GFP mice administering scFv-Bsec

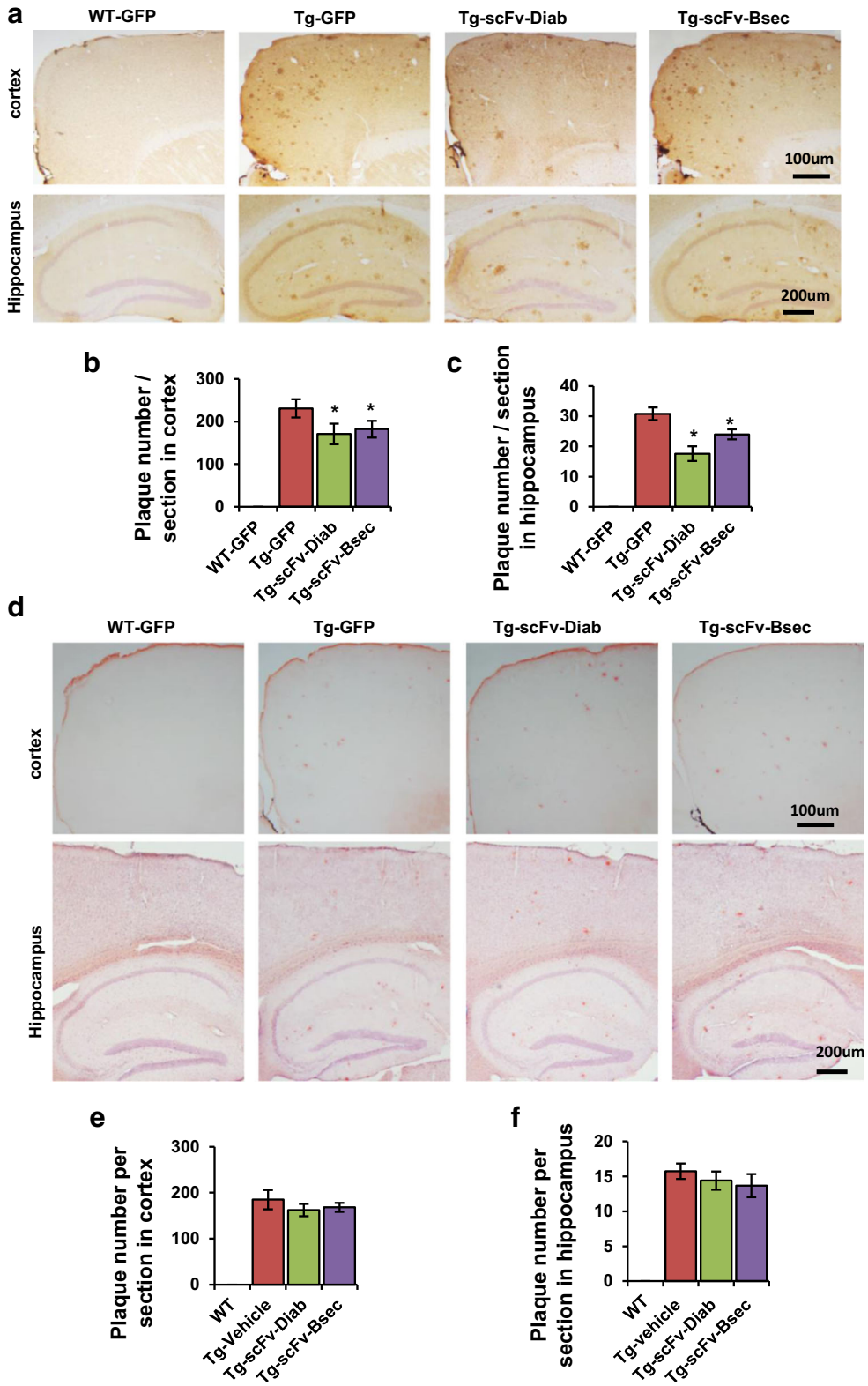

Fig. 3 Amyloid β deposits in the brain sections of APP/PS1 mice. **a** Representative microphotoimages showed Aβ deposits demonstrated by specific antibody 6E10 staining in the cortex (upper) and the hippocampus (bottom). Counterstaining by hemotaxylin. **b** The number of 6E10-positive deposits was counted and shown per section in the cortex tissue. **c** Similar to **b**, the data was shown per section in the hippocampus. **d** Representative microphotoimages showed fibrillar deposits demonstrated by Congo red histostaining in the cortex (upper) and the hippocampus (bottom). Counterstaining by hemotaxylin. **e** The number of Congo red–positive deposits was counted and shown per section in the cortex. **f** Similar to **e**, the data was shown per section in the hippocampus. Data are based on the following group sizes: scFv-Diab ($n = 9$), scFv-Bsec ($n = 6$), Tg-GFP ($n = 10$), and WT-GFP ($n = 3$). *$p < 0.05$ to vehicle Tg-GFP mice

Both scFv-Diab and scFv-Bsec Decrease Aβ Deposits in APP/PS1 Mice

The amyloidogenic pathway for processing APP generates Aβ which ultimately accumulates in the parenchyma [22]. Amyloid plaque accumulation is observed in the cortex and the hippocampus in the transgenic mice but not the wild-type mice (Fig. 3a). The number of 6E10-positive plaques was decreased in the cortex and the hippocampus of mice treated with scFv-Bsec or scFv-Diab compared with the GFP control group (Fig. 3b, $*p < 0.05$). The number of Congo red–positive water-insoluble fibril plaques in the cortex of the control GFP-treated transgenic mice (Congo red positive, 185.6 ± 21.0) was lower than the number of 6E10-stained amyloid plaques (6E10 positive, 230.8 ± 21.5) (Fig. 3b, d) as was the number of Congo red deposits (Congo red positive, 15.7 ± 1.1) in the hippocampus compared with 6E10-stained amyloid deposits (6E10 positive, 30.8 ± 2.1) (Fig. 3c, f). Treatment with scFv-Bsec or scFv-Diab did not significantly decrease the number of Congo red–positive deposits in the cortex (Fig. 3e, $p > 0.05$) or the hippocampus (Fig. 3f, $p > 0.05$), indicating that the scFv-Bsec and scFv-Diab reduce formation of soluble amyloid aggregates but not insoluble fibrillar formation.

Both scFv-Diab and scFv-Bsec Lowered Oligomeric Aβ Levels in APP/PS1 Mice

Since the scFv-Bsec and scFv-Diab reduced generation of soluble amyloid β, we next determined if the treatments could reduce generation of toxic oligomeric Aβ species. We used two different scFvs previously generated in our lab, A4 [27] and C6T [28], to assay for the presence of different oligomeric Aβ species as described previously [29–31]. Results showed a significant elevation in the levels of A4- and C6T-specific oligomers in the cortex and the hippocampus of transgenic vehicle mice compared with age-matched WT mice (Fig. 4a, b, $^{###}p < 0.001$). Treatment with scFv-Bsec and scFv-Diab lowered A4-reactive oligomeric Aβ levels in the cortex and the hippocampus, compared with vehicle transgenic mice (Fig. 4a, $*p < 0.05$). Similarly, C6T-recognized oligomeric Aβ levels were reduced in the mice treated with scFv-Diab and scFv-Bsec (Fig. 4b, $*p < 0.05$).

Both scFv-Diab and scFv-Bsec Decrease Gliosis and Microgliosis in APP/PS1 Mice

High levels of Aβ burden may be cytotoxic, activate glial cells, and lead to altered inflammatory responses [22, 23]. To assess the effects of scFv-Bsec and scFv-Diab treatment on inflammation, we assayed levels of GFAP-positive reactive astrocytes. The presence of activated astrocytes correlates with the presence of Congo red–positive plaques in the cortex (Fig. 5a) and there is a significant increase in activated astrocytes in transgenic vehicle mice compared with age-matched WT mice (Fig. 5b, $^{###}p < 0.001$). Similar results were observed in the hippocampus (Fig. 5c, d, $^{###}p < 0.001$). Neither treatment with scFv-Bsec or scFv-Diab resulted in a significant decrease in reactive astrocytes in the cortex (Fig. 5b, $p > 0.05$) though both treatments did reduce activation in the hippocampus (Fig. 5d, $*p < 0.05$).

Microglia activation is another response to toxic substrates [22, 23]. The double immunostaining was performed using antibody Iba1, a microglial marker, and 6E10 as an Aβ marker. Representative images showed a correlation of Iba1-positive cells with 6E10-labeling Aβ plaques (Fig. 5e). A significant increase in the number of activated microglia was

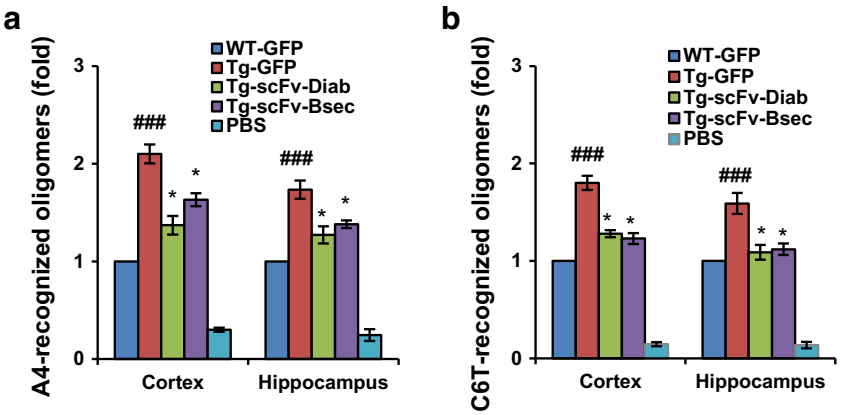

Fig. 4 Oligomeric Aβ levels in the brain of APP/PS1 mice. **a** Oligomeric Aβ levels were measured using antibody scFv A4 by ELISA. **b** Oligomeric Aβ levels were measured using antibody scFv C6T by ELISA. Data was expressed as ratio to wild-type (vehicle WT-GFP mice) in the cortex and hippocampus, respectively. The numbers of mice used for each study were as follows: scFv-Diab ($n = 9$), scFv-Bsec ($n = 6$), Tg-GFP ($n = 10$), and WT-GFP ($n = 3$). PBS was considered as a blank sample control. $^{###}p < 0.001$ to age-matched WT-GFP mice; $*p < 0.05$ to vehicle Tg-GFP mice

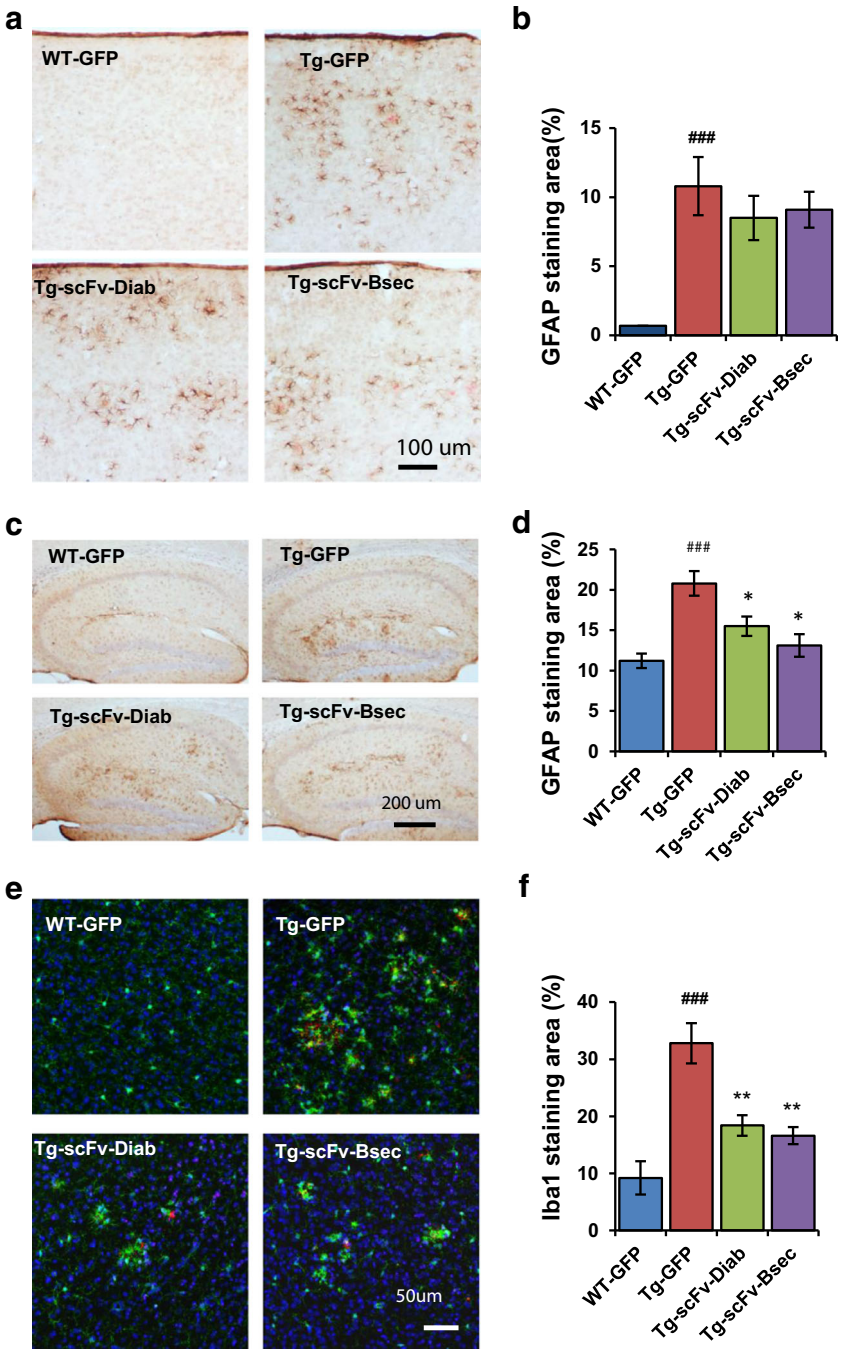

Fig. 5 Gliosis reaction responsive to Aβ in the brain of APP/PS1 mice. **a** Representative microphotoimages showed reactive astrocytes immunostained by antibody against GFAP. Fibrillar Aβ deposits were visualized by Congo red staining (red). The nuclei were counterstained with hematoxylin (blue). **b** The positive staining of reactive astrocytes was expressed as a percentage of total area. **c** Similar to **a**, representative microphotoimages in the hippocampus. **d** The positive staining of reactive astrocytes was expressed as a percentage of total area. **e** Representative microphotoimages showed reactive microglia immunostained by antibody Iba1 (green). Aβ deposits were visualized by antibody 6E10 (red). Counterstaining by DAPI (blue). **f** The positive staining of microglia was expressed as a percentage of total area. Group size tested: scFv-Diab ($n = 5$), scFv-Bsec ($n = 5$), Tg-GFP ($n = 5$), and WT-GFP ($n = 3$). $^{\#\#}p < 0.01$, $^{\#\#\#}p < 0.001$ to age-matched WT-GFP mice; $^{**}p < 0.01$ to littermate Tg-GFP vehicle group

observed in transgenic vehicle mice compared with age-matched WT mice (Fig. 5f, $^{\#\#\#}p < 0.001$). Treatment with both scFv-Bsec and scFv-Diab significantly reduced reactive microglia in the cortex (Fig. 5F, $^{**}p < 0.01$).

scFv-Diab But Not scFv-Bsec Reversed Dendrite Spine Loss and Synaptic Aggregates

The number of the dendrites of pyramidal neurons decreases in APP-based transgenic mouse models of AD [23, 32, 33]. Dendritic density and organization were imaged using MAP-2 staining. Compared with WT mice, the transgenic GFP-treated mice had higher staining of MAP2 and a decreased number of MAP2-positive dendrites and spines (Fig. 6a, b, $^{\#\#}p < 0.01$). Treatment with scFv-Diab rescued dendritic organization similar to the vehicle WT mice and increased the number of MAP2-positive staining compared with the transgenic vehicle mice (Fig. 6B, $^{*}p < 0.05$). Treatment with scFv-Bsec however did not rescue dendritic organization or increase

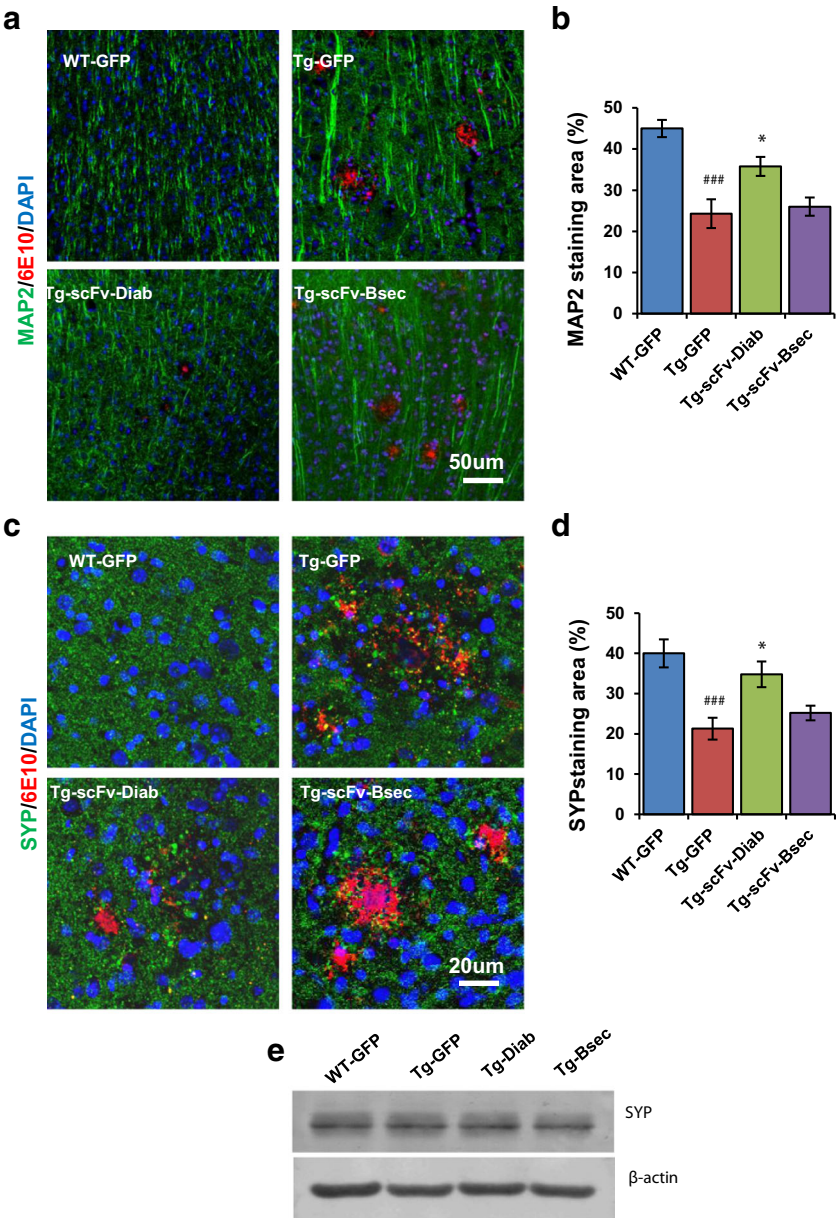

Fig. 6 Changes in dendritic spines and synapses in the brain of APP/PS1 mice. **a** Representative microphotoimages showed neuronal dendrites in the cortex visualized by an antibody against MAP2 (green). Aβ deposits were visualized by antibody 6E10 (red). Counterstaining by DAPI (blue). **b** The area of positive MAP2-labeled dendrites was expressed as a percentage of total area. **c** Representative microphotoimages showed synapses labeled by an antibody against SYP (green). Aβ deposits were visualized by antibody 6E10 (red). Counterstaining by DAPI (blue). **d** The area of positive SYP staining was expressed as a percentage of total area. **e** Representative data showing SYP levels in the cortex by Western blot. Group size tested: scFv-Diab ($n = 5$), scFv-Bsec ($n = 5$), Tg-GFP ($n = 5$), and WT-GFP ($n = 3$). $^{\#\#}p < 0.01$, $^{\#\#\#}p < 0.001$ to age-matched WT-GFP mice; $^{**}p < 0.01$ to littermate Tg-GFP vehicle group

MAP2 staining (Fig. 6a, b, $p > 0.05$). Synaptic changes in the treated mice were also characterized using synaptophysin (SYP, a pre-synaptic marker). Strong staining of neuritic aggregates close to 6E10-positive plaques was observed in the cortex of transgenic GFP control mice compared with wild-type mice (Fig. 6c, d, $^{\#\#}p < 0.01$). Treatment with scFv-Diab significantly decreased the number of SYP aggregates (strong staining) around Aβ plaques (Fig. 6c, d, $^{*}p < 0.05$). Treatment with scFv-Bsec however did not significantly change the number of SYP-positive aggregates close to Aβ plaques (Fig. 6c, d, $p > 0.05$). In total, synaptophysin levels were not unchanged in the different treated groups as determined by Western blot (Fig. 6e).

ScFv-Diab Improves Neurogenesis

Processing of APP can affect neurogenesis as evidenced by the decline in neurogenesis in APP transgenic models of AD [34]. We tracked changes in neurogenesis using doublecortin (DCX), a classical marker for immature neurons [34, 35]. Positive staining was observed in the subgranular zone (SGZ) of the dentate gyrus of the hippocampus (Fig. 7a) where the transgenic vehicle treated mice showed a significant decrease compared with similarly treated WT mice (Fig. 7b, $^{\#\#}p < 0.01$). Treatment with scFv-Diab increased the number of DCX-positive cells in the SGZ to levels much higher than even the WT mice (Fig. 7b, $^{***}p < 0.001$). Treatment with iBsec1 also

increased the number of immature neurons compared with WT mice (Fig. 7b, $^{**}p < 0.01$) but the levels were significantly lower than the mice treated with scFv-Diab (Fig. 7b, $^{\&\&\&}p < 0.001$).

ScFv-Diab But Not scFv-Bsec Rescues Survival in APP/PS1 Mice

All mice were purchased at an age of 1 month and housed following standard IACUC protocols. While 10 WT mice were housed for 9 months with no loss of mice, the APP/PS1 mice have a high mortality rate, around 40% by the age of 12 months [36]. Consistent with these reports, 20 APP/PS1 mice were randomly chosen and injected with rAAV-GFP at age of 1 month old as a vehicle group but only 10 mice had survived after 9 months (Fig. 8). The iBsec1-treated mice showed a slight delay but no change in total mortality, whereas the Diab-treated mice quite strikingly increased survival levels to nearly wild-type levels, where only one mouse died (Fig. 8).

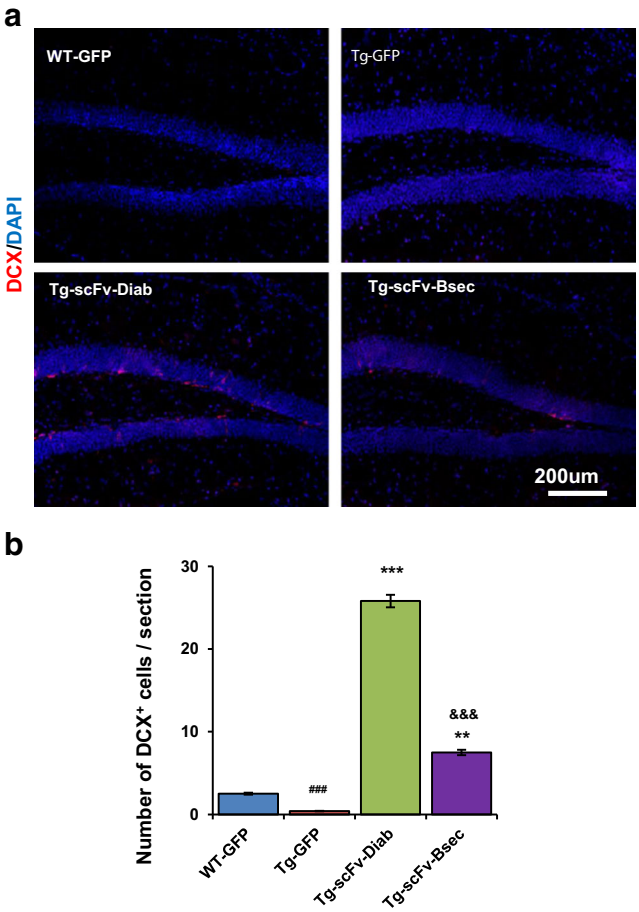

Fig. 7 Neurogenesis in the brain of APP/PS1 mice. **a** Representative microphotoimages show immature neurons in SGZ of the hippocampus using an antibody against DCX (red). Counterstaining by DAPI (blue). **b** DCX-positive cells were counted and averaged per sections. Group size tested: scFv-Diab ($n = 9$), scFv-Bsec ($n = 6$), Tg-GFP ($n = 10$), and WT-GFP ($n = 5$). $^{###}p < 0.001$ to age-matched WT-GFP mice. $^{**}p < 0.01$, $^{***}p < 0.001$ to littermate Tg-GFP vehicle group; $^{\&\&\&}p < 0.001$ to Tg-GFP mice administering scFv-Diab

Discussion

We previously generated two scFvs, Asec1 and iBsec1, which respectively promote α-secretase activity and block β-secretase activity toward APP by binding to APP at either the α-site or the β-site [15, 18, 37]. We generated a tandem bispecific scFv (diabody or Diab) that combines the Asec1 and iBsec1 scFvs into a single construct and showed that it elevates levels of sAPPα, a soluble α-secretase-associated APP fragment, and decreases levels of Aβ and sAPPβ, a soluble β-secretase-associated fragment in cell models of AD [19]. Here, we added an LDL receptor which can facilitate transfer across the blood-brain barrier (BBB) [20, 38, 39] to the Diab and iBsec1 constructs for their use in animal models of AD. Using recombinant human adeno-associated virus (rAAV) as a vector infective to hepatic cells, the tagged constructs could be secreted into the blood and then cross the BBB into the brain. We found high levels of both scFv-Diab and scFv-Bsec in treated mouse brain tissue. The constructs were tested as therapeutics in an APP/PS1 AD model. Treatment with scFv-Bsec reduced levels of sAPPβ as expected and treatment with scFv-Diab also increased sAPPα levels significantly higher than in the control mice and the scFv-Bsec-treated mice ($^{\&\&\&}p < 0.001$), indicating that the diabody simultaneously inhibits β-secretase processing and promotes α-secretase activity.

Consistent with the decreased levels of sAPPβ, we found decreased 6E10-positive Aβ deposits in both the scFv-Bsec-

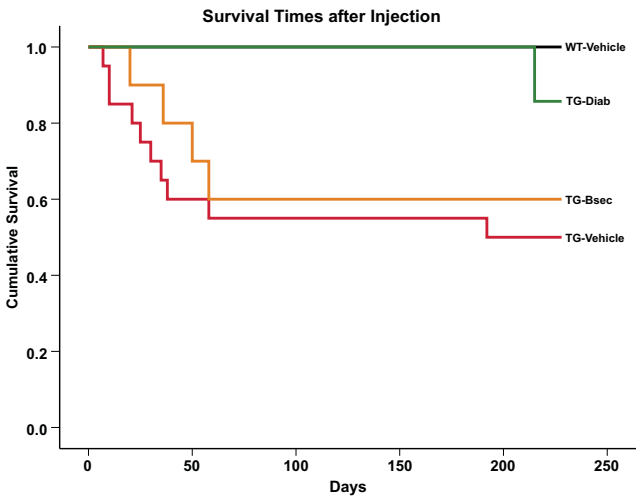

Fig. 8 Survival comparison among the mice. Mice with scFv-Diab had a higher survival rate, similar to WT-GFP vehicle mice, compared with the mice in scFv-Bsec administration and Tg-GFP vehicle group

and scFv-Diab-treated mice, although insoluble Congo red–stained amyloid deposits did not decrease. To further study how soluble aggregates were affected by the treatments, we measured levels of two conformationally distinct oligomeric Aβ variants using the A4 and C6T scFvs previously generated by our group [27, 28]. It is not clear why soluble Aβ aggregates are decreased with treatment, but not insoluble aggregates, though various scenarios such as different aggregation pathways or locations could account for the difference. Astrocytosis- and microgliosis-based inflammation in the brains correlates strongly with the neurodegenerative process in AD [40] and the presence of activated astrocytes and microglia around neuritic plaques is one of the hallmarks of Aβ-related neuropathological progression [41, 42]. An increase in GFAP-positive astrocytes was also observed with clustering of hypertrophic Iba1-positive microglia around amyloid deposits [22, 23]. Treatment with scFv-Diab and scFv-Bsec significantly decreased the number of astrocytes in the hippocampus but not in the cortex. This difference may reflect regional differences in Aβ deposition which was shown to start earlier in the cortex (1.5 months) than in the hippocampus (4 months) [23].

Dendritic spine loss and synaptic pathology are common characteristics of APP/PS1 mice [23, 32, 33] as is clustering of SYP-labeled synaptic buttons [23, 32]. Treatment with scFv-Diab restored MAP2-labeled dendrite spine density and synapse organization in the cortex compared with vehicle treated mice, although treatment with iBsec1 did not improve either MAP2 or SYP organization. Treatment with scFv-Diab also greatly elevated neurogenesis in the hippocampus of APP/PS1 mice. Most dramatically however, the high mortality rate of the APP/PS1 was rescued in the scFv-Diab-treated mice, but not the iBsec1-treated mice. Both scFv-Bsec and scFv-Diab reduce β-site cleavage of APP, resulting in similar decreases in sAPPβ, A4- and C6T-recognizing Aβ oligomers, 6E10-positive Aβ deposit, and microgliosis. However, the Diab also promotes α-secretase cleavage generating higher levels of sAPPα which was shown to protect hippocampal neurons from excitotoxicity and Aβ toxicity [43, 44], stimulate proliferation of adult progenitor cells [45, 46], reduce deregulation of NMDA receptor [47], and antagonize dendritic degeneration and neuron death [48]. It is likely that the increase in sAPPα production at least partially accounts for the increased neuronal health and dramatically increased survival rates in the scFv-Diab-treated mice.

A clinical trial testing verubecestat, a BACE1 inhibitor, as a treatment in mild to moderate AD patients was recently canceled due to futility [13]. Our results here provide encouraging evidence that while inhibiting BACE activity may not be effective, altering APP processing is still a promising therapeutic strategy. Treatment with scFv-Bsec, which inhibits BACE processing of APP, showed a decrease in plaque deposition and inflammation, but did not improve neuronal health nor increase survival rates. However, treatment with scFv-Diab, which simultaneously decreases amyloidogenic processing by inhibiting β-secretase activity while also promoting neuroprotective processing by promoting α-secretase activity, similarly decreased plaques and inflammation, and also restored neuronal health and dramatically increased survival rates. Simultaneously inhibiting β-secretase activity while promoting α-secretase activity has promise as a novel therapeutic approach for treating AD and other APP-related disorders including Down's syndrome.

Acknowledgements We thank Dr. Hailan Yao from the Roskamp Institute for providing some of antibodies.

Funding Information This work was supported in part by grants from the National Institutes of Health, Alzheimer's Association, and the AZTE Catalyst Fund.

Compliance with Ethical Standards

All protocols for animal use were approved by the Institutional Animal Care and Use Committee (IACUC) of the Arizona State University at Tempe, Arizona. Experiments described here were carried out in accordance with good animal practice following NIH recommendations.

Conflict of Interest M Sierks is a founder of Studio Biotherapeutics.

References

1. Hardy J, Selkoe DJ (2002) The amyloid hypothesis of Alzheimer's disease: progress and problems on the road to therapeutics. Science 297(5580):353–356. https://doi.org/10.1126/science.1072994
2. Kumar D, Ganeshpurkar A, Kumar D, Modi G, Gupta SK, Singh SK (2018) Secretase inhibitors for the treatment of Alzheimer's disease: long road ahead. Eur J Med Chem 148:436–452. https://doi.org/10.1016/j.ejmech.2018.02.035
3. Mullard A (2017) BACE inhibitor bust in Alzheimer trial. Nat Rev Drug Discov 16(3):155. https://doi.org/10.1038/nrd.2017.43
4. Gu K, Li Q, Lin H, Zhu J, Mo J, He S, Lu X, Jiang X et al (2017) Gamma secretase inhibitors: a patent review (2013 - 2015). Expert Opin Ther Pat 27(7):851–866. https://doi.org/10.1080/13543776.2017.1313231
5. Golde TE, Koo EH, Felsenstein KM, Osborne BA, Miele L (2013) gamma-Secretase inhibitors and modulators. Biochim Biophys Acta 1828(12):2898–2907. https://doi.org/10.1016/j.bbamem.2013.06.005
6. Doody RS, Raman R, Farlow M, Iwatsubo T, Vellas B, Joffe S, Kieburtz K, He F et al (2013) A phase 3 trial of semagacestat for treatment of Alzheimer's disease. N Engl J Med 369(4):341–350. https://doi.org/10.1056/NEJMoa1210951
7. Hunt CE, Turner AJ (2009) Cell biology, regulation and inhibition of beta-secretase (BACE-1). FEBS J 276(7):1845–1859. https://doi.org/10.1111/j.1742-4658.2009.06929.x
8. Kim DY, Gersbacher MT, Inquimbert P, Kovacs DM (2011) Reduced sodium channel Na(v)1.1 levels in BACE1-null mice. J Biol Chem 286(10):8106–8116. https://doi.org/10.1074/jbc.M110.134692
9. Sankaranarayanan S, Price EA, Wu G, Crouthamel MC, Shi XP, Tugusheva K, Tyler KX, Kahana J et al (2008) In vivo beta-

secretase 1 inhibition leads to brain Abeta lowering and increased alpha-secretase processing of amyloid precursor protein without effect on neuregulin-1. J Pharmacol Exp Ther 324(3):957–969. https://doi.org/10.1124/jpet.107.130039
10. von Arnim CA, Kinoshita A, Peltan ID, Tangredi MM, Herl L, Lee BM, Spoelgen R, Hshieh TT et al (2005) The low density lipoprotein receptor-related protein (LRP) is a novel beta-secretase (BACE1) substrate. J Biol Chem 280(18):17777–17785. https://doi.org/10.1074/jbc.M414248200
11. Hu X, He W, Diaconu C, Tang X, Kidd GJ, Macklin WB, Trapp BD, Yan R (2008) Genetic deletion of BACE1 in mice affects remyelination of sciatic nerves. FASEB J 22(8):2970–2980
12. Wang H, Song L, Laird F, Wong PC, Lee HK (2008) BACE1 knock-outs display deficits in activity-dependent potentiation of synaptic transmission at mossy fiber to CA3 synapses in the hippocampus. J Neurosci 28(35):8677–8681
13. Egan MF, Kost J, Tariot PN, Aisen PS, Cummings JL, Vellas B, Sur C, Mukai Y et al (2018) Randomized trial of verubecestat for mild-to-moderate Alzheimer's disease. N Engl J Med 378(18):1691–1703. https://doi.org/10.1056/NEJMoa1706441
14. Lee M, Bard F, Johnson-Wood K, Lee C, Hu K, Griffith SG, Black RS, Schenk D et al (2005) Abeta42 immunization in Alzheimer's disease generates Abeta N-terminal antibodies. Ann Neurol 58(3):430–435
15. Boddapati S, Levites Y, Sierks MR (2011) Inhibiting beta-secretase activity in Alzheimer's disease cell models with single-chain antibodies specifically targeting APP. J Mol Biol 405(2):436–447. https://doi.org/10.1016/j.jmb.2010.10.054
16. Fahrenholz F (2007) Alpha-secretase as a therapeutic target. Curr Alzheimer Res 4(4):412–417
17. Kasturirangan S, Boddapati S, Sierks MR (2010) Engineered proteolytic nanobodies reduce Abeta burden and ameliorate Abeta-induced cytotoxicity. Biochemistry 49(21):4501–4508. https://doi.org/10.1021/bi902030m
18. Kasturirangan S, Brune D, Sierks M (2009) Promoting alpha-secretase cleavage of beta-amyloid with engineered proteolytic antibody fragments. Biotechnol Prog 25(4):1054–1063. https://doi.org/10.1002/btpr.190
19. Boddapati S, Levites Y, Suryadi V, Kasturirangan S, Sierks MR (2012) Bispecific tandem single chain antibody simultaneously inhibits beta-secretase and promotes alpha-secretase processing of AbetaPP. J Alzheimers Dis 28(4):961–969. https://doi.org/10.3233/JAD-2011-111196
20. Spencer B, Emadi S, Desplats P, Eleuteri S, Michael S, Kosberg K, Shen J, Rockenstein E et al (2014) ESCRT-mediated uptake and degradation of brain-targeted alpha-synuclein single chain antibody attenuates neuronal degeneration in vivo. Mol Ther 22(10):1753–1767. https://doi.org/10.1038/mt.2014.129
21. Spencer BJ, Verma IM (2007) Targeted delivery of proteins across the blood-brain barrier. Proc Natl Acad Sci 104(18):7594–7599. https://doi.org/10.1073/pnas.0702170104
22. Jankowsky JL, Fadale DJ, Anderson J, Xu GM, Gonzales V, Jenkins NA, Copeland NG, Lee MK et al (2004) Mutant presenilins specifically elevate the levels of the 42 residue beta-amyloid peptide in vivo: evidence for augmentation of a 42-specific gamma secretase. Hum Mol Genet 13(2):159–170. https://doi.org/10.1093/hmg/ddh019
23. Radde R, Bolmont T, Kaeser SA, Coomaraswamy J, Lindau D, Stoltze L, Calhoun ME, Jaggi F et al (2006) Abeta42-driven cerebral amyloidosis in transgenic mice reveals early and robust pathology. EMBO Rep 7(9):940–946. https://doi.org/10.1038/sj.embor.7400784
24. He P, Zhong Z, Lindholm K, Berning L, Lee W, Lemere C, Staufenbiel M, Li R et al (2007) Deletion of tumor necrosis factor death receptor inhibits amyloid beta generation and prevents learning and memory deficits in Alzheimer's mice. J Cell Biol 178(5):829–841. https://doi.org/10.1083/jcb.200705042
25. He P, Cheng X, Staufenbiel M, Li R, Shen Y (2013) Long-term treatment of thalidomide ameliorates amyloid-like pathology through inhibition of beta-secretase in a mouse model of Alzheimer's disease. PLoS One 8(2):e55091. https://doi.org/10.1371/journal.pone.0055091
26. He P, Liu Q, Wu J, Shen Y (2012) Genetic deletion of TNF receptor suppresses excitatory synaptic transmission via reducing AMPA receptor synaptic localization in cortical neurons. FASEB J 26(1):334–345. https://doi.org/10.1096/fj.11-192716
27. Zameer A, Kasturirangan S, Emadi S, Nimmagadda SV, Sierks MR (2008) Anti-oligomeric Abeta single-chain variable domain antibody blocks Abeta-induced toxicity against human neuroblastoma cells. J Mol Biol 384(4):917–928. https://doi.org/10.1016/j.jmb.2008.09.068
28. Kasturirangan S, Reasoner T, Schulz P, Boddapati S, Emadi S, Valla J, Sierks MR (2013) Isolation and characterization of antibody fragments selective for specific protein morphologies from nanogram antigen samples. Biotechnol Prog 29(2):463–471. https://doi.org/10.1002/btpr.1698
29. Kasturirangan S, Li L, Emadi S, Boddapati S, Schulz P, Sierks MR (2012) Nanobody specific for oligomeric beta-amyloid stabilizes nontoxic form. Neurobiol Aging 33(7):1320–1328. https://doi.org/10.1016/j.neurobiolaging.2010.09.020
30. Williams SM, Schulz P, Rosenberry TL, Caselli RJ, Sierks MR (2017) Blood-based oligomeric and other protein variant biomarkers to facilitate pre-symptomatic diagnosis and staging of Alzheimer's disease. J Alzheimers Dis 58:23–35. https://doi.org/10.3233/jad-161116
31. Williams SM, Schulz P, Sierks MR (2015) Oligomeric alpha-synuclein and beta-amyloid variants as potential biomarkers for Parkinson's and Alzheimer's diseases. Eur J Neurosci 43:3–16. https://doi.org/10.1111/ejn.13056
32. Bittner T, Burgold S, Dorostkar MM, Fuhrmann M, Wegenast-Braun BM, Schmidt B, Kretzschmar H, Herms J (2012) Amyloid plaque formation precedes dendritic spine loss. Acta Neuropathol 124(6):797–807. https://doi.org/10.1007/s00401-012-1047-8
33. Liebscher S, Page RM, Kafer K, Winkler E, Quinn K, Goldbach E, Brigham EF, Quincy D et al (2014) Chronic gamma-secretase inhibition reduces amyloid plaque-associated instability of pre- and postsynaptic structures. Mol Psychiatry 19(8):937–946. https://doi.org/10.1038/mp.2013.122
34. He P, Staufenbiel M, Li R, Shen Y (2014) Deficiency of patched 1-induced Gli1 signal transduction results in astrogenesis in Swedish mutated APP transgenic mice. Hum Mol Genet 23(24):6512–6527. https://doi.org/10.1093/hmg/ddu370
35. He P, Shen Y (2009) Interruption of beta-catenin signaling reduces neurogenesis in Alzheimer's disease. J Neurosci 29(20):6545–6557. https://doi.org/10.1523/JNEUROSCI.0421-09.2009
36. Gimbel DA, Nygaard HB, Coffey EE, Gunther EC, Lauren J, Gimbel ZA, Strittmatter SM (2010) Memory impairment in transgenic Alzheimer mice requires cellular prion protein. J Neurosci 30(18):6367–6374. https://doi.org/10.1523/JNEUROSCI.0395-10.2010
37. Rangan SK, Liu R, Brune D, Planque S, Paul S, Sierks MR (2003) Degradation of beta-amyloid by proteolytic antibody light chains. Biochemistry 42(48):14328–14334. https://doi.org/10.1021/bi035038d
38. Spencer B, Marr RA, Gindi R, Potkar R, Michael S, Adame A, Rockenstein E, Verma IM et al (2011) Peripheral delivery of a CNS targeted, metalo-protease reduces abeta toxicity in a mouse model of Alzheimer's disease. PLoS One 6(1):e16575. https://doi.org/10.1371/journal.pone.0016575
39. Spencer B, Verma I, Desplats P, Morvinski D, Rockenstein E, Adame A, Masliah E (2014) A neuroprotective brain-penetrating

endopeptidase fusion protein ameliorates Alzheimer disease pathology and restores neurogenesis. J Biol Chem 289(25):17917–17931. https://doi.org/10.1074/jbc.M114.557439

40. Maccioni RB, Rojo LE, Fernandez JA, Kuljis RO (2009) The role of neuroimmunomodulation in Alzheimer's disease. Ann N Y Acad Sci 1153:240–246. https://doi.org/10.1111/j.1749-6632.2008.03972.x
41. Yan Q, Zhang J, Liu H, Babu-Khan S, Vassar R, Biere AL, Citron M, Landreth G (2003) Anti-inflammatory drug therapy alters beta-amyloid processing and deposition in an animal model of Alzheimer's disease. J Neurosci 23(20):7504–7509
42. Simard AR, Soulet D, Gowing G, Julien JP, Rivest S (2006) Bone marrow-derived microglia play a critical role in restricting senile plaque formation in Alzheimer's disease. Neuron 49(4):489–502. https://doi.org/10.1016/j.neuron.2006.01.022
43. Furukawa K, Sopher BL, Rydel RE, Begley JG, Pham DG, Martin GM, Fox M, Mattson MP (1996) Increased activity-regulating and neuroprotective efficacy of alpha-secretase-derived secreted amyloid precursor protein conferred by a C-terminal heparin-binding domain. J Neurochem 67(5):1882–1896
44. Barger SW, Harmon AD (1997) Microglial activation by Alzheimer amyloid precursor protein and modulation by apolipoprotein E. Nature 388(6645):878–881. https://doi.org/10.1038/42257
45. Caille I, Allinquant B, Dupont E, Bouillot C, Langer A, Muller U, Prochiantz A (2004) Soluble form of amyloid precursor protein regulates proliferation of progenitors in the adult subventricular zone. Development 131(9):2173–2181. https://doi.org/10.1242/dev.01103
46. Demars MP, Bartholomew A, Strakova Z, Lazarov O (2011) Soluble amyloid precursor protein: a novel proliferation factor of adult progenitor cells of ectodermal and mesodermal origin. Stem Cell Res Ther 2(4):36. https://doi.org/10.1186/scrt77
47. Moreno L, Rose C, Mohanraj A, Allinquant B, Billard JM, Dutar P (2015) sAbetaPPalpha improves hippocampal NMDA-dependent functional alterations linked to healthy aging. J Alzheimers Dis 48(4):927–935. https://doi.org/10.3233/JAD-150297
48. Copanaki E, Chang S, Vlachos A, Tschape JA, Muller UC, Kogel D, Deller T (2010) sAPPalpha antagonizes dendritic degeneration and neuron death triggered by proteasomal stress. Mol Cell Neurosci 44(4):386–393. https://doi.org/10.1016/j.mcn.2010.04.007